Supporting Information:

Inkjet-printed transparent micro-supercapacitors with morphology tailored co-continuous mesoporous Mn_3O_4

Sushree Sangita Priyadarsini[a], Suryansh Saxena[a, †], Jyoti Ranjan Pradhan[a], Subho Dasgupta[a,*]

[a]Department of Materials Engineering, Indian Institute of Science (IISc), C V Raman Avenue, Bangalore: 560012, Karnataka, India

[†]Current affiliation: Department of Material Science and Engineering, University of California, San Diego, USA

[*]Email: dasgupta@iisc.ac.in

Keywords: Flexible electronics; Inkjet printing; Transparent micro-supercapacitors

Content:

A. Transmission electron micrograph of printed Mn_3O_4 thin film

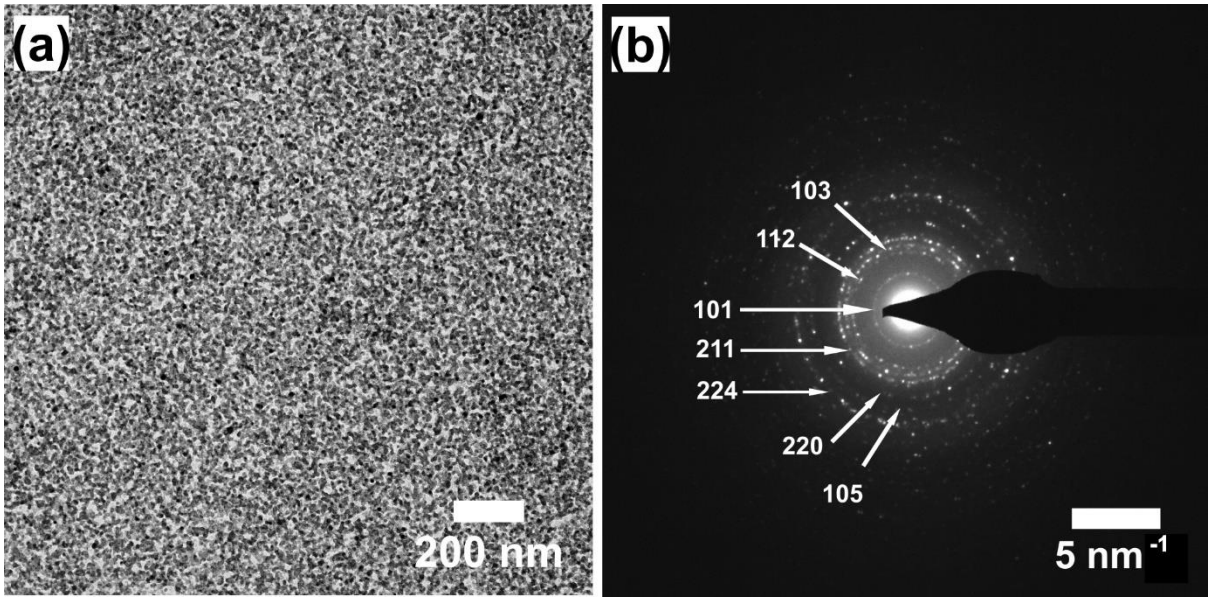

Figure S1 (a) Transmission electron micrograph, and (b) Selected area electron diffraction of the printed and annealed active material ink with all the planes matching with Mn_3O_4.

B. Scanning tunnelling electron microscopy images of printed Mn_3O_4 thin film

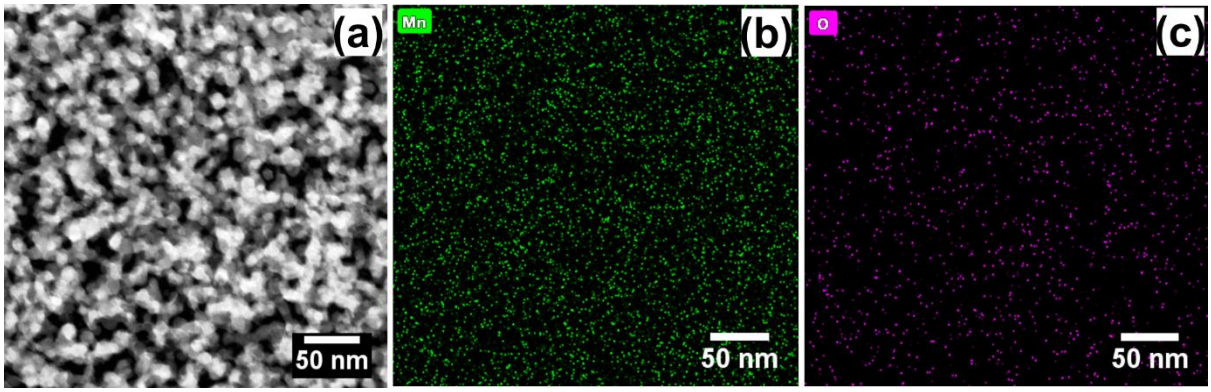

Figure S2 (a) STEM image of printed and annealed active material showing co-continuous mesoporous structure, (b) and (c) show manganese and oxygen signal from EDX elemental mapping performed at STEM mode.

C. Cyclic voltammogram of drop-cast electrodes under 3-electrode measurement setup

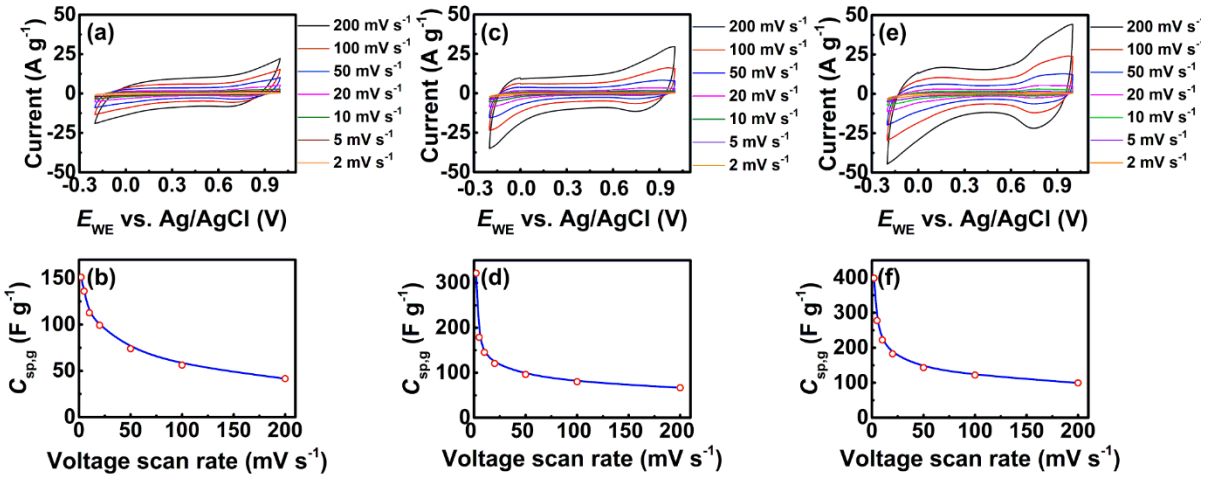

Figure S3 Electrochemical characterization of the drop-cast Mn_3O_4 electrodes using 3-electrode setup, and with respect to Ag/AgCl as the reference electrode. (a) Cyclic voltammogram of 0.3 M ink-based Mn_3O_4 electrode, (b) Calculated gravimetric specific capacitance of the 0.3 M ink-based electrode as a function of voltage scan rate, (c) Cyclic voltammogram of 0.06 M ink based Mn_3O_4 electrode, (d) Gravimetric specific capacitance of the 0.06 M ink-based electrode as a function of voltage scan rate, (e) Cyclic voltammogram of 0.03 M ink based Mn_3O_4 electrode, (b) Gravimetric specific capacitance of the 0.03 M ink-based electrode as a function of voltage scan rate.

D. Galvanostatic (chrono-potentiometric) charge/discharge measurements of drop-cast electrodes under 3-electrode measurement setup

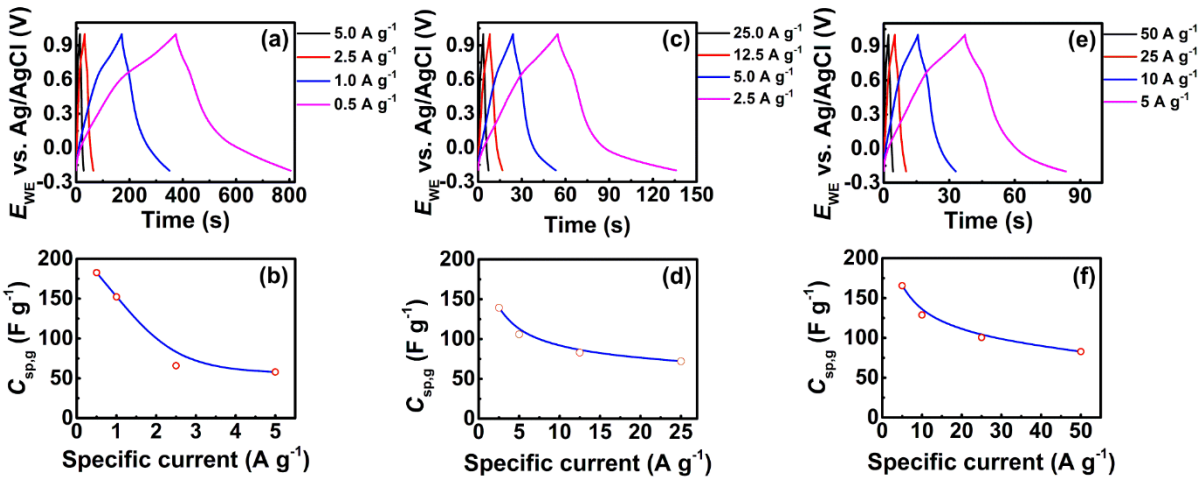

Figure S4 Electrochemical characterization of the drop-cast Mn_3O_4 electrodes using 3-electrode setup and with respect to Ag/AgCl as the reference electrode. (a) GCD curves of 0.3 M ink-based Mn_3O_4 electrode, (b) Gravimetric specific capacitance of the 0.3 M ink-based Mn_3O_4 electrode as a function of specific current, (c) GCD curve of 0.06 M ink-based Mn_3O_4 electrode, (d) Gravimetric specific capacitance of the 0.06 M ink-based Mn_3O_4 electrode as a function of specific current, (e) GCD curve of 0.03 M ink based Mn_3O_4 electrode, (b) Gravimetric specific capacitance of the 0.03 M ink-based Mn_3O_4 electrode as a function of specific current.

E. Capacitance comparison for different concentration of Mn_3O_4 ink estimated with 3-electrode measurement setup

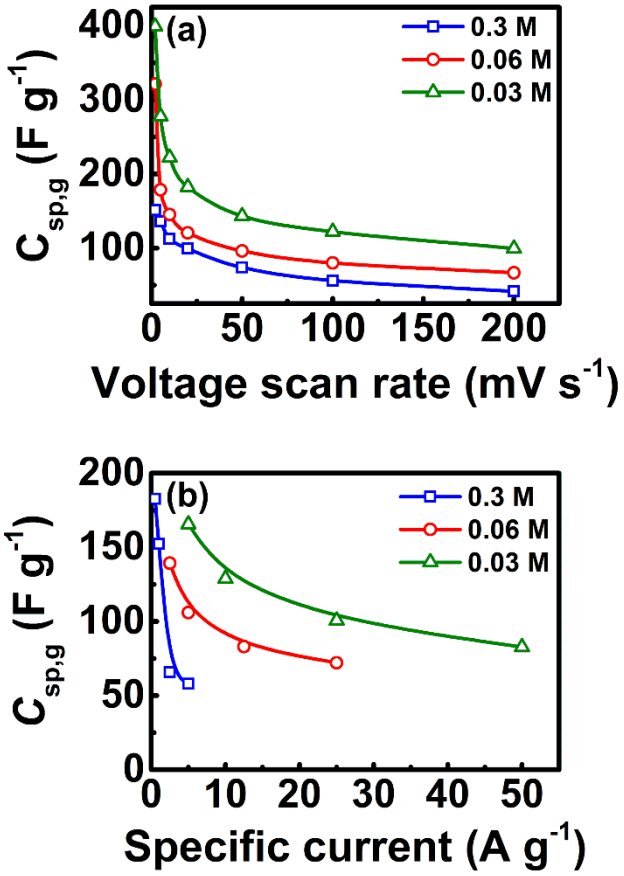

Figure S5 Comparison of estimated capacitance values of the Mn_3O_4 electrode prepared with inks of three different concentrations that are, 0.3 M, 0.06 M and 0.03 M under the 3-electrode setup with respect to Ag/AgCl as the reference electrode. (a) Comparative gravimetric specific capacitance as a function of the voltage scan rate and (b) Comparative gravimetric specific capacitance as a function of specific current.

F. Schematic to understand the change in mechanism of charge storage from drop cast to printed electrode with 0.3 M ink

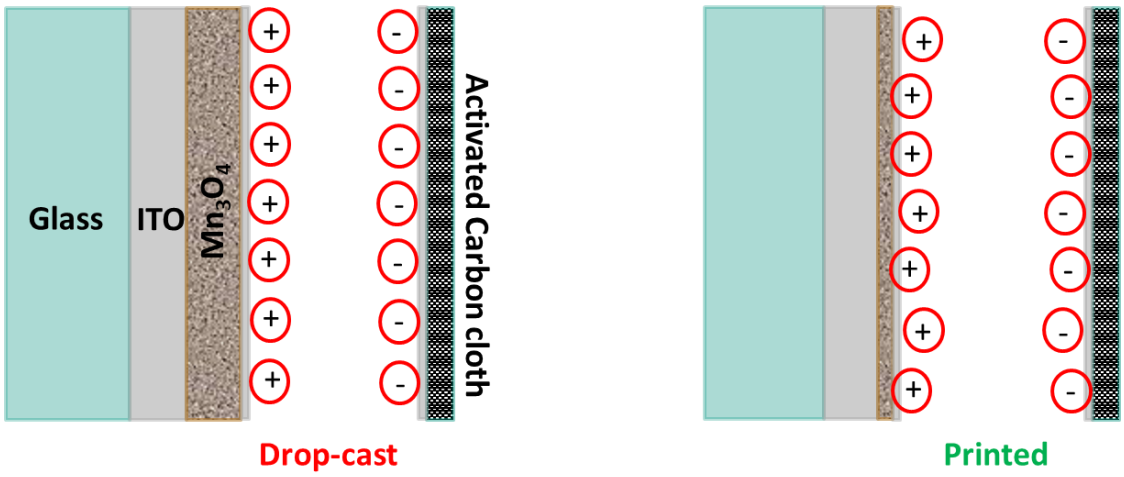

Figure S6 The proposed reason behind different mechanism of charge storage with changing fabrication protocol of electrode from drop cast to printing. The thickness as well as the porosity does not remain constant when the fabrication protocol is changed from drop cast to printing with 0.3 M ink.

G. Nyquist plot of the printed symmetric MSC with water-based and DMSO-based electrolytes

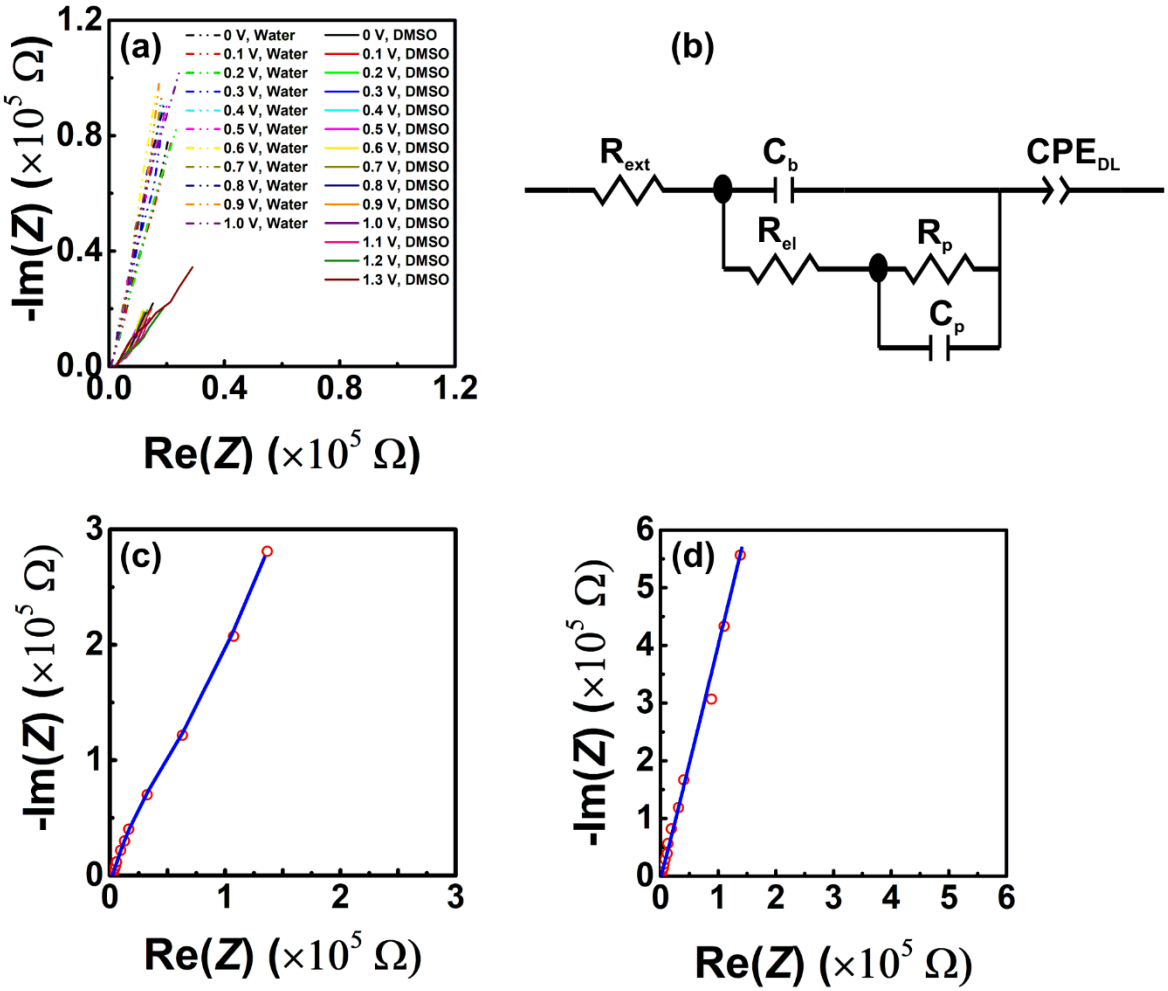

Figure S7 The measured differential impedance spectroscopy data showing (a) the Nyquist plots of the symmetric MSC with water based (dash-dot lines) and DMSO based (solid line) CSPE measured at various applied DC potential between 0 V to 1 V and 0 V to 1.3 V, respectively; (b) equivalent circuit diagram that has been used to fit the Nyquist plots (c) DMSO based, (d) water based MSC, measured at 0 V, applied DC bias; the red dots are the experimental data points and the and blue solid line is fit using the equivalent circuit shown in (b).

In Figure S7b, we have assumed an electrical circuit, where R_{ext}, R_{el} and R_p are the external resistance, bulk electrolyte resistance and the resistance towards pseudocapacitive charge storage or the charge transfer resistance, respectively. The R_{el} has been considered in parallel to the bulk capacitance of the solvent of the electrolyte, C_b. The *RC*-circuit corresponding to the bulk electrolytic behaviour has been considered to be in series with the external resistance of the MSC. On the other hand, the resistance to pseudocapacitive charge storage has been kept in parallel to the pseudocapacitance C_p. The constant phase element CPE_{DL} assumed here takes care of the EDL capacitance along with the huge porosity of the electrode material and also the surface states that may be present and causing local variations in conductivity.

H. Comparison of cyclic-voltammogram measured with DMSO-based electrolyte having $LiClO_4$ and $NaClO_4$ as the supporting electrolytes

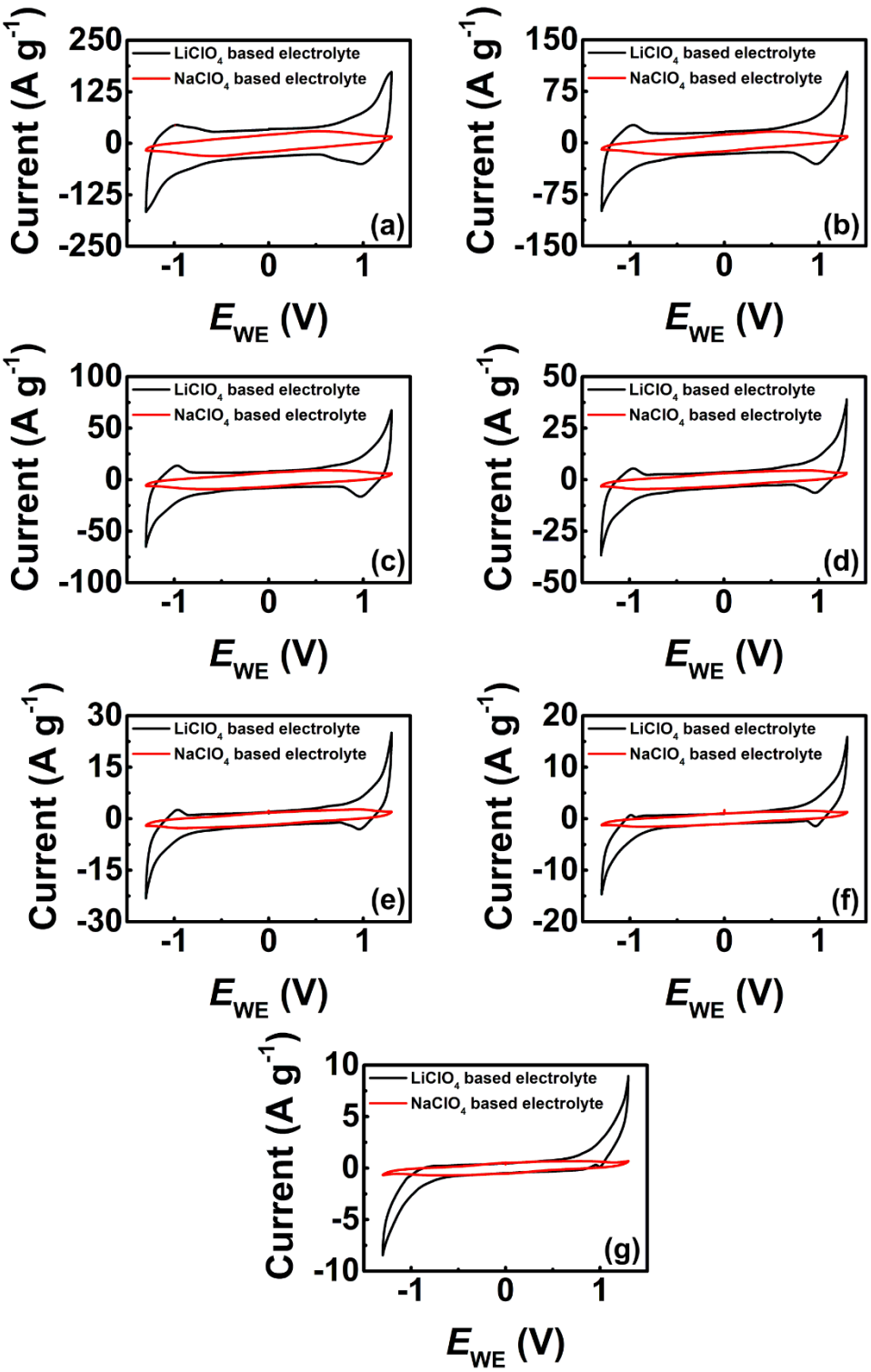

Figure S8 Comparison of cyclic voltammograms of printed all solid Mn_3O_4 (ink with 0.3 M concentration) based transparent microsupercapacitors with non-aqueous (DMSO) based solid electrolyte having $LiClO_4$ and $NaClO_4$ as the supporting electrolytes for a potential window of -1.3 V to 1.3 V under 2-electrode setup and measured with voltage scan rate of (a) 200 mV s^{-1}, (b) 100 mV s^{-1}, (c) 50 mV s^{-1}, (d) 20 mV s^{-1}, (e) 10 mV s^{-1}, (f) 5 mV s^{-1}, and (g) 2 mV s^{-1}.

I. Scanning electron micrograph of mesoporous Mn_3O_4 film in as-printed and annealed condition and after 5000 galvanostatic charge/discharge cycles.

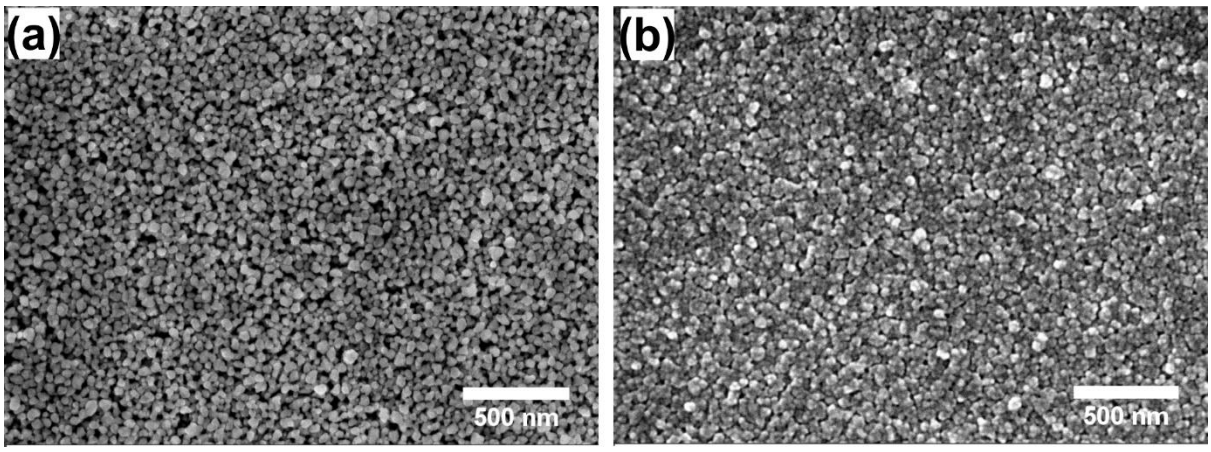

Figure S9 SEM images of (a) printed and annealed mesoporous Mn_3O_4 layer, (b) mesoporous Mn_3O_4 electrode layer after 5000 galvanostatic charge-discharge cycles.

The comparative surface morphology analysis before and after the galvanostatic charge-discharge cycles indicates that a nominal surface reconstruction of the Mn_3O_4 electrode material may have happened. Such surface reconstruction after a large number of cycles is well-known for battery electrodes, and here in the present case, it can be also expected for the intercalation-type pseudocapacitive microsupercapacitor electrodes.

J. Scanning electron micrograph of the Mn_3O_4 film on Au coated Kapton before and after the dynamic mechanical (bending fatigue) test

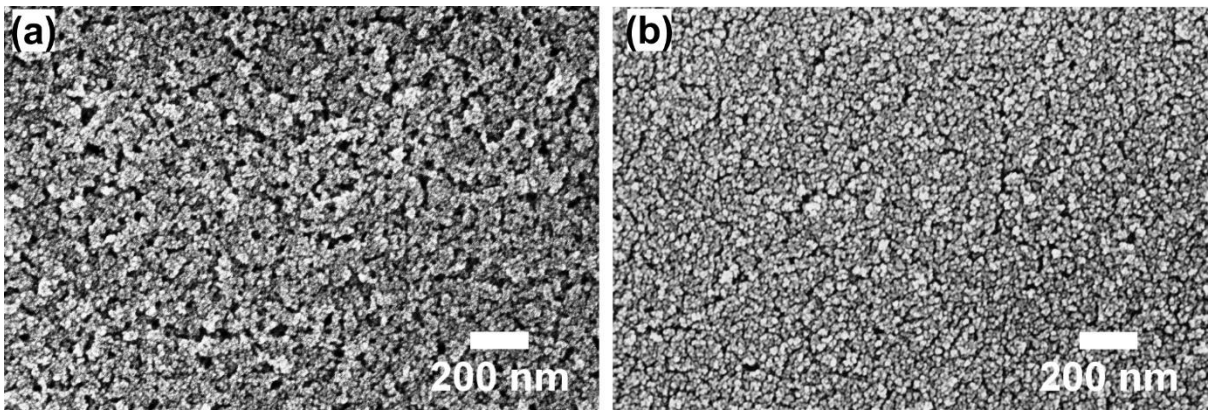

Figure S10 Comparison of the scanning electron micrograph of the printed Mn_3O_4 film on Au coated Kapton (a) before and (b) after mechanical bending fatigue tests with bending diameter of 10 mm.

K. Atomic force micrographs of mesoporous Mn_3O_4 film in as-printed and annealed condition and after 100 complete bending fatigue test cycles.

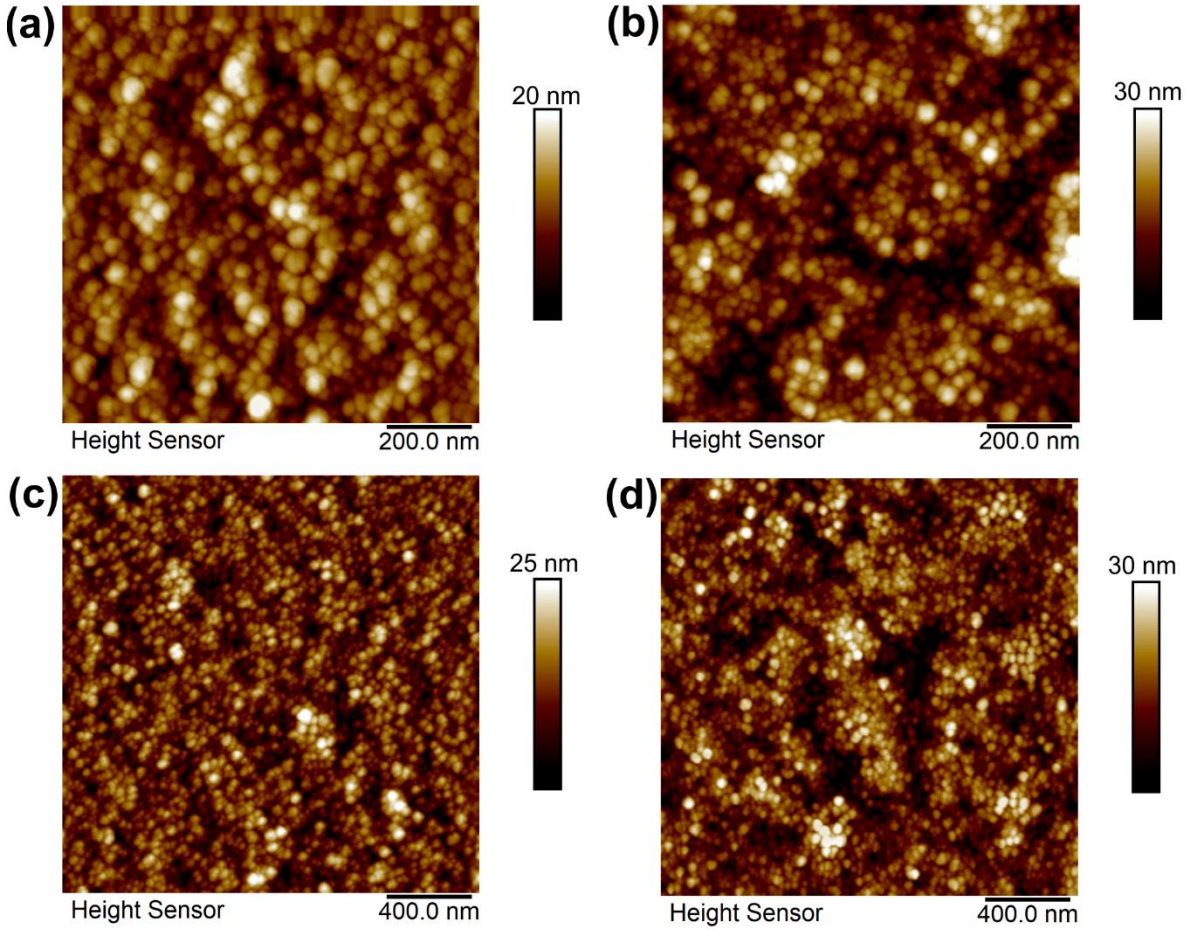

Figure S11 Atomic force micrograph of mesoporous Mn_3O_4 film (a,c) in as-printed and annealed condition, and (b,d) after 100 complete bending fatigue test cycles. Frames (a,b) show 1×1 μm^2, and frames (c,d) show 2×2 μm^2 area on the Mn_3O_4 film surface, respectively.

The AFM images taken on mesoporous Mn3O4 film after the bending fatigue test appear to have noticeable microcracks, and an increased overall surface roughness. For example, the RMS surface roughness value for the 1×1 μm^2 frame size AFM image increased from 2.97 nm for the as-prepared film (Figure S11a) to 5.35 nm after the bending fatigue test (Figure S11b).

L. Comparison of the present work with literature reports of Mn_3O_4 and inkjet-printed supercapacitors

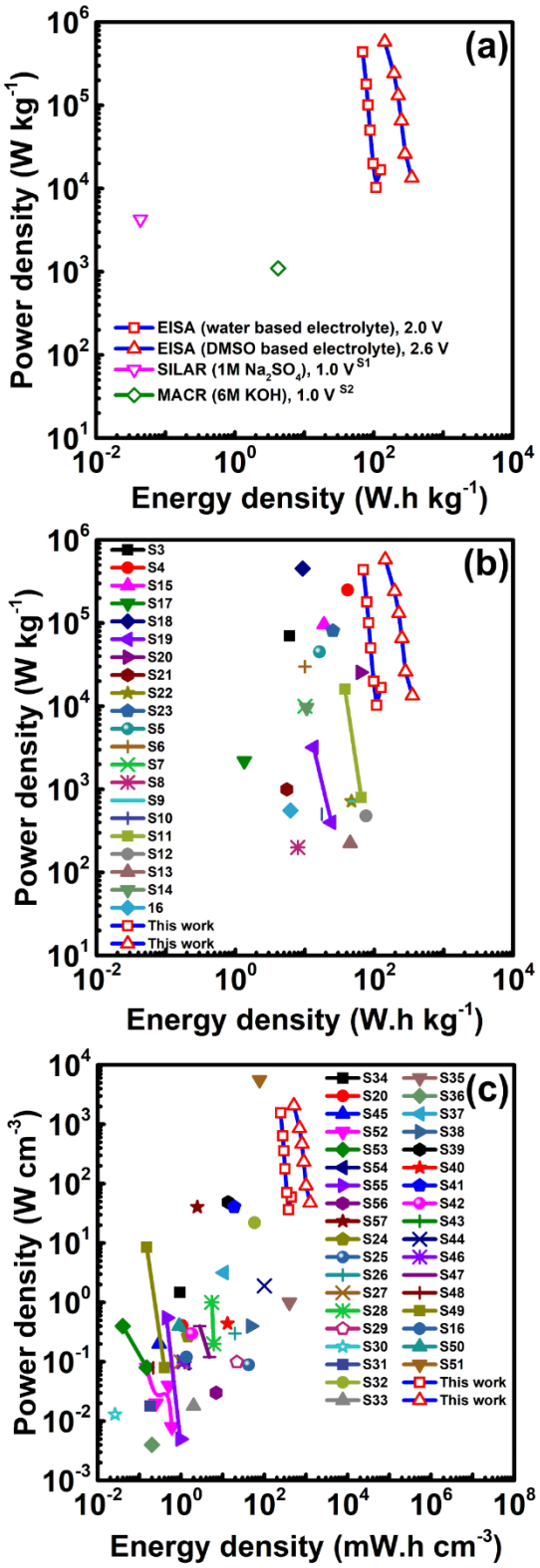

Fig. S12. (a) Ragone plot of the printed micro-supercapacitor at potential window of 2 V (water based solid electrolyte) and 2.6 V (DMSO based solid electrolyte) in comparison with the previously reported symmetric Mn_3O_4 supercapacitors, fabricated by successive ionic layer adsorption and reaction (SILAR) method,[S1] and by a microwave-assisted chemical route

(MACR).[S2] (b) Ragone plot with gravimetric energy density and power density of the previously reported printed supercapacitor in comparison to the present work;[S3–S23] and (c) Ragone plot with volumetric energy density and power density of the previously reported printed supercapacitor in comparison to the present work. [S16, S20, S24–S57]

The energy and power density of the present inkjet-printed planar symmetric micro-supercapacitors have been compared with the previously reported symmetric supercapacitors based on Mn_3O_4 and is shown in a Ragone plot presented in Fig. S10a. The inkjet-printed symmetric MSC shows high energy density as well as power density as compared to the previously reported Mn_3O_4 based symmetric supercapacitors owing to the high surface-to-volume ratio of co-continuous mesoporous microstructure and homogeneous film formation with controlled delivery of ink volume with inkjet printing. The Ragone plot showing the gravimetric and volumetric energy density and power density of the present printed MSC is also compared with other printed micro-supercapacitors involving wide range of electrode materials that have been reported in the literature and is summarized in Fig. S10b and S10c, respectively. This comparative viewgraphs show that the inkjet-printed MSCs with co-continuous mesoporous electrode architecture, demonstrated in the present study, offers excellent gravimetric and volumetric values when compared to the literature data, either involving previous reports on Mn_3O_4 electrodes, or earlier work on printed micro-supercapacitors that have used carbon based on other high conducting or pseudocapacitive electrode materials.

M. Galvanostatic (chrono-potentiometric) charge/discharge measurements of the flexible MSC before and after the dynamic mechanical (bending fatigue) test

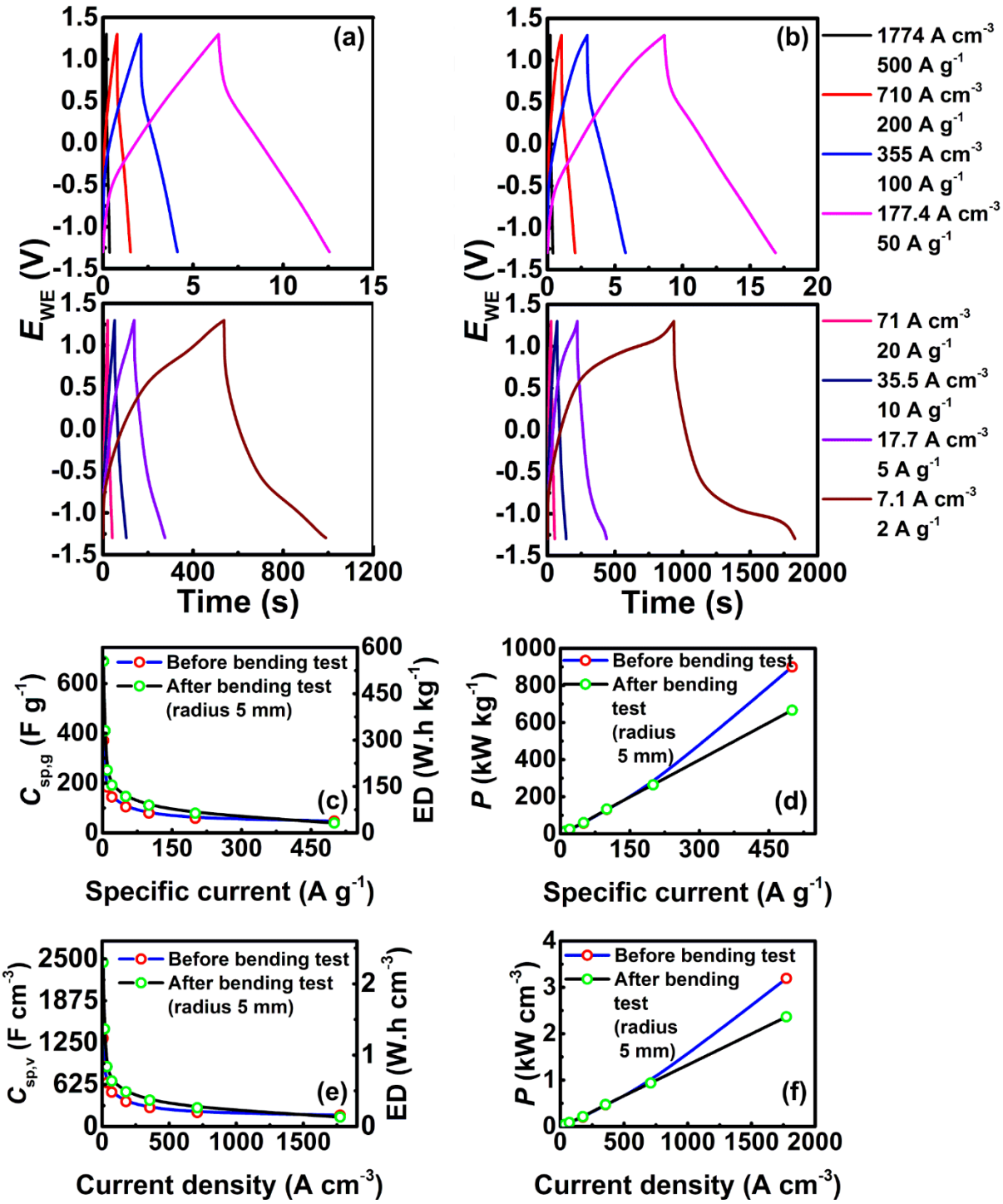

Fig. S13. The galvanostatic charge/discharge plots of the flexible MSC on kapton substrate before and after the mechanical bending fatigue test and all parameters calculated from the GCD curves. (a) Galvanostatic charge/discharge with varying current before mechanical bending fatigue test; (b) Galvanostatic charge/discharge with varying current after mechanical bending fatigue test with bending radius of 5 mm; Comparison of (c) Specific gravimetric capacitance and energy density, (d) power density as a function of specific current, (e) Specific volumetric capacitance and energy density, and (f) power density as a function of current density, before and after the dynamic bending test.

N. Table S1 Comparison of the present work with literature reports of Mn_3O_4 supercapacitors

Material details	Fabrication method	Processing temperature (°C)	Measurement technique	Max. capacitance		Electrolyte used	Ref.
				3 electrode	2 electrode		
Mn_3O_4 lamellae+19 % C	Electrochemical deposition	RT	CV	145 F g^{-1} at 2 mV s^{-1}		Aqueous KCl	S58
Mn_3O_4 film	Electrostatic spray deposition	200	CV	330 F g^{-1} at 50 mV s^{-1}		0.1 M Na_2SO_4	S59
Mn_3O_4 powder	Hydrothermal	120	CV	170 F g^{-1} at 500 mV s^{-1}		1 M Na_2SO_4	S60
Mn_3O_4 film	Chemical bath deposition	80	CV	193 F g^{-1} at 10 mV s^{-1}		1 M Na_2SO_4	S61
Mn_3O_4 powder	Hydrothermal	180	CV	322 F g^{-1} at 5 mV s^{-1}		1 M Na_2SO_4	S62
Mn_3O_4 film	Chemical bath deposition	RT	CV	284 F g^{-1} at 5 mV s^{-1}		1M Na2SO4	S63
Mn_3O_4 film	Successive ionic layer absorption and reaction	RT	CV	314 F g^{-1} at 5 mV s^{-1}		1 M Na_2SO_4	S64
Mn_3O_4 powder	Hydrothermal	200	CV	148 F g^{-1} at 5 mV s^{-1}		2 M KCl	S65
Mn_3O_4 film	SILAR	RT	CV		72 F g^{-1} at 5 mV s^{-1} (at 70 °C)	1 M Na_2SO_4	S1
Mn_3O_4 film	Chemical bath deposition	70	CV	398 F g^{-1} at 5 mV s^{-1}		1 M Na_2SO_4	S66
Mn_3O_4 powder	Sol-gel method	350	CP		30.8 F g^{-1} at 50 mA g^{-1}	1 M Li_2SO_4	S67
Mn_3O_4 powder	Ultrasonic process	RT	CP	262 F g^{-1} at 0.4 A g^{-1}		1 M Na_2SO_4	S68
Mn_3O_4 powder	Pulsed laser deposition	RT	CV	120 F g^{-1} at 100 mV s^{-1}		1 M Na_2SO_4	S69
Mn_3O_4 powder	Microwave-assisted two-step chemical method	300	CV		1330.16 F g^{-1} at 0.01 mV s^{-1}	6 M KOH	S2
Mn_3O_4 nanofibers	Electrospinning	350	CV	190 F g^{-1} at 3 mV s^{-1}		1 M KCl	S70
Mn_3O_4 powder	Hydrothermal	150	CP	348 F g^{-1} at 0.5 mA cm^{-2}		1 M Na_2SO_4	S71
Mn_3O_4 powder	Chemical precipitation method	RT	CP	348 F g^{-1} at 0.5 mA cm^{-2}		1 M Na_2SO_4	S72
Amorphous porous Mn_3O_4	Electrodeposition method	100	CV		3.05 F cm^{-3} at 5 mV s^{-1}	1 M NaOH, PVA	S73
Mn_3O_4 cubes	Sol-gel method	500	CV	667 F g^{-1} at 1 mV s^{-1}		6 M KOH	S74
Porous Mn_3O_4 thin film	Spray pyrolysis	350	CV	394 F g^{-1} at 10 mV s^{-1}		1 M Na_2SO_4	S75
Mn_3O_4 film	Electron beam evaporation	-	CV		535 F cm^{-3} at 2 mV s^{-1}	LiCl + PVA	S76

Mn_3O_4 powder	Hydrothermal	150	CV	198 F g^{-1} at 0.5 mA cm^{-2}		0.5 M Li_2SO_4	S77
Mn_3O_4 beaded chains	Electro-spinning process	1000	CP	445 F g^{-1} at 0.5 A g^{-1}		1 M Na_2SO_4	S78
Mn_3O_4 film	Electron beam evaporation	500	CP	568 F g^{-1} at 1 A g^{-1}		1 M Na_2SO_4	S79
Mn_3O_4 nanoparticles	Co-precipitation method	RT	CP	260 F g^{-1} at 1 A g^{-1}		1 M Na_2SO_4	S80
Mn_3O_4 nanoparticles	Ultrasonic irradiation assisted co-precipitation method	120	CP	296 F g^{-1} at 1 A g^{-1}		3M KOH	S81
Mn_3O_4 film	**Evaporation Induced Self Assembly**	**400**	**CV**	**1201 F g^{-1} at 2 mV s^{-1}**	**2411 F cm^{-3}, 679.5 F g^{-1} at 2 mV s^{-1}**	**1M aq. LiCl (3-electrode), DMSO + $LiClO_4$ based gel (MSC)**	**This work**

O. Table S2 Comparison of gravimetric energy and power density of present work with previously reported printed supercapacitors that are available in the literature.

Material	Fabrication method	Potential window (V)	Energy density (W.h kg^{-1})	Power density (W kg^{-1})	Ref.
SWCNT, $LiPF_6$/EC:DEC	Spray coating	3	6	70000	S3
CNT, $LiPF_6$/EC:DEC	Inkjet Printing	3	41.25	250000	S4
SWCNT + RuO_2 nanowire, PVA/H_3PO_4	Inkjet Printing	1	18.8	96000	S15
Graphene oxide nanosheet, 1M H_2SO_4	Inkjet Printing	1	1.34	2190	S17
NGP/PANI, 1M H_2SO_4	Screen Printing	1	9.3	454000	S18
Graphene, Polyaniline	Inkjet Printing	0.8	24.02, 13.29	400.33, 3202.4	S19
Graphene Oxide, $EMIMBF_4$	Direct printing	3.5	63	25500	S20
Graphene, $EMIMBF_4$	Inkjet Printing	3	5.5	1000	S21
Au/MnO_x nanocone	Contact-printing	1.8	46.8	720	S22
MnO_2, LiCl/PVA	Direct Printing	0.8	25.3	81000	S23
MWCNT, [EMIM][BF_4] gel	Inkjet Printing	3	16.2	45000	S5
Activated carbon/CNT, [BMIM][BF_4]/ETPTA	Inkjet Printing	2	10	30000	S6
Graphene oxide, PVA/H_2SO_4 gel	Inkjet Printing	0.8	10	10000	S7
SWCNT + PANI, PVA/H_3PO_4	Spray printing	0.8	7.9	200	S8
MnO_2/T-PANI, porous carbon, 1 M Na_2SO_4	Stencil printing	1.8	52.7	720	S9
MnO_2/Ag, PVA/KOH	Inkjet Printing	1	17.5	500.95	S10
$Ni(OH)_2$/RGO + AC, KOH soaked PTFE	Inkjet Printing	1.6	37.7, 64.8	16000, 800	S11
Ni-Co LDH/Ag/rGO on CC, KOH soaked paper	Inkjet Printing	1.6	76	480	S12
Graphene/CoS_2/Ni_3S_4, PVA/KOH	Screen printing	1.5	44.9	224.8	S13
Mesoporous WO_3/NiO, $LiClO_4$ + propylene carbonate	Printing	2.3	10.6	9600	S14
Graphene/Mn_3O_4/EC/CNT, PVDF/$LiClO_4$	Direct printing	0.8	6.19	556.7	S16
Mn_3O_4, PVA/LiCl	**Inkjet printing**	**2**	**125**	**438726**	**This work**
Mn_3O_4, PVA/$LiClO_4$/DMSO	**Inkjet printing**	**2.6**	**353**	**581412**	

P. Table S3 Comparison of volumetric energy and power density of present work with previously reported printed supercapacitors that are available in the literature.

Material	Fabrication method	Potential window (V)	Energy density (mW.h cm^{-3})	Power density (W cm^{-3})	Ref.
Polyacrylonitrile, $EMIMBF_4$	Spin-on nanoprinting (SNAP)	3	0.94	1.48	S34
Graphene Oxide, $EMIMBF_4$	Direct printing	3.5	1.06	0.408	S20
Nitrogen doped reduced graphene oxide	Screen Printing	0.8	0.3	0.2	S45
MnO2/onion-like carbon, PVA:H_3PO_4	Screen Printing	0.8	0.6, 0.5, 0.25, 0.15	0.008, 0.04, 0.02, 0.08	S52
Graphene, Na_2SO_4:PVA	Stencil printing	0.8	0.15, 0.04	0.08, 0.4	S53
MnO_2 + CNT/Ag nanoparticle, 4 M LiCl	Inkjet Printing	1.8	1.28	0.096	S54
$(K_2Co_3(P_2O_7)_2.2H_2O$ whiskers+ graphene nanosheets,	Inkjet Printing	1.07	0.96, 0.45	0.005, 0.55	S55
Graphene, PVA-H_2SO_4 gel	micro-extrusion printing	1	7	0.03	S56
Graphene, PVA/H_3PO_4 gel	Inkjet Printing	1	2.47	40.3	S57
V_2O_5/CNT, PVA/LiCl	Facile Printing	0.8	1.47	0.27	S24
PEDOT:PSS-CNT/Ag, PVA/H_3PO_4	Inkjet printing	0.9	42.1	0.089	S25
Graphene, $EMIMBF_4$ ionic liquid	Spray printing	4	19.6	0.3	S26
Graphene	Inkjet printing	1	1	0.1	S27
$Ti_3C_2T_x$, PVA/H_3PO_4	Laser printing	0.6	5.48–6.10	0.2-1	S28
Graphene oxide + MnO_2, PVA/LiCl	Inkjet printing	1	22	0.099	S29
Graphene, KI/ H_2SO_4	Spray printing	1.2	0.026	0.013	S30
δ-MnO_2, PVA/LiCl	Screen printing	0.8	0.18	0.018	S31
Nitrogen doped nanoporous carbon, PVA/H2SO4	Contact printing	0.8	58	22	S32
RGO/MoO_3, PVA/H2SO4 gel	Inkjet printing	0.8	2	0.018	S33
NiO, PVA/KOH gel	Inkjet printing	1.5	400	1	S35
Graphene, Nanographene oxide/H_3PO_4	Inkjet printing	1	0.2	0.004	S36
Graphene/CNT, PVA/H_3PO_4	Screen printing	1	10.7	3.17	S37
MoO_3 nanorods, Na-alginate hydrogel	Screen printing	2.8	47.11	0.4	S38
RuO2 on $Ti_3C_2T_x$, PVA/KOH gel	Screen printing	0.6	13.5	48.5	S39
MnO_2@C/VN, $MgSO_4$-PAM gel	Screen printing	2.4	13.1	0.44	S40
$RuO_2.xH_2O$ NP/AgNW/GO, PVA/KOH gel	Screen printing	2	18.8	40.9	S41
Graphene, $EMIMNTF_2$ IL	Screen printing	2.7	1.81	0.297	S42
Fe–MnO_2 nanosheet, PVA/LiCl	Inkjet printing	1	1.13	0.11	S43

$Ti_3C_2T_x$ MXene, PVA/H_2SO_4 gel	Inkjet printing	1	100.2	1.9	[S44]
Graphene, PVA/H_2SO_4 gel	Inkjet printing	1	1.2	0.1	[S46]
PANI, PVA/H_2SO_4 gel	Laser printing	0.8	2.8, 4.8	0.4, 0.12	[S47]
MoS_2, PVA/H_2SO_4 gel	Inkjet printing	0.8	0.215	0.079	[S48]
MOF-199@ZIF-67/C, H_2SO_4	Laser printing	1	0.4, 0.15	0.08, 9	[S49]
Graphene/Mn_3O_4/EC/CNT, PVDF/$LiClO_4$	Direct printing	0.8	1.35	0.12	[S16]
Nitrogen doped carbon, PVA/H_2SO_4 gel	Inkjet printing	1	0.9	0.4	[S50]
RGO@PANI, PVA/H_2SO_4 gel	Inkjet printing	1	76.94	5593.7	[S51]
Mn_3O_4, PVA/LiCl	**Inkjet printing**	**2**	**440**	**1557**	**This work**
Mn_3O_4, PVA/$LiClO_4$/DMSO	**Inkjet printing**	**2.6**	**1250**	**2063**	

References

S1 D. P. Dubal, A. D. Jagadale and C. D. Lokhande, *Electrochim. Acta*, 2012, **80**, 160–170.

S2 V. C. Bose and V. Biju, *Bull. Mater. Sci.*, 2015, **38**, 865–873.

S3 M. Kaempgen, C. K. Chan, J. Ma, Y. Cui and G. Gruner, *Nano Lett.*, 2009, **9**, 1872–1876.

S4 L. Hu, H. Wu and Y. Cui, *Appl. Phys. Lett.*, 2010, **96**, 1–4.

S5 S. K. Ujjain, P. Ahuja, R. Bhatia and P. Attri, *Mater. Res. Bull.*, 2016, **83**, 167–171.

S6 K. H. Choi, J. T. Yoo, C. K. Lee and S. Y. Lee, *Energy Environ. Sci.*, 2016, **9**, 2812–2821.

S7 Z. Pei, H. Hu, G. Liang and C. Ye, *Nano-Micro Lett.*, 2017, **9**, 1–11.

S8 R. Wang, Q. R. Wang, M. J. Yao, K. N. Chen, X. Y. Wang, L. L. Liu, Z. Q. Niu and J. Chen, *Rare Met.*, 2018, **37**, 536–542.

S9 L. Jia, L. Zheng, W. Wang, Y. Shi, Q. Zhang and X. Xu, *Mater. Lett.*, 2019, **252**, 80–83.

S10 T. Cheng, Y. Wu, Y. Chen, Y. Zhang, W. Lai and W. Huang, *Small*, 2019, **15**, 1901830.

S11 X. Li, R. Chen, Y. Zhao, Q. Liu, J. Liu, J. Yu, J. Li, P. Liu, J. Li and J. Wang, *Chem. Eng. J.*, , DOI:10.1016/j.cej.2019.121988.

S12 X. Li, Y. Zhao, J. Yu, Q. Liu, R. Chen, H. Zhang, D. Song, R. Li, J. Liu and J. Wang, *J. Colloid Interface Sci.*, 2019, **557**, 691–699.

S13 D. Jiang, H. Liang, W. Yang, Y. Liu, X. Cao, J. Zhang, C. Li, J. Liu and J. J. Gooding, *Carbon N. Y.*, 2019, **146**, 557–567.

S14 K.-W. Kim, T. Y. Yun, S.-H. You, X. Tang, J. Lee, Y. Seo, Y.-T. Kim, S. H. Kim, H. C. Moon and J. K. Kim, *NPG Asia Mater.*, 2020, **12**, 84.

S15 P. Chen, H. Chen, J. Qiu and C. Zhou, *Nano Res.*, 2010, **3**, 594–603.

S16 M. L. Seol, E. Sadatian, S. Jang, C. Hill, I. Nam, J. W. Han and M. Meyyappan, *ACS Appl. Electron. Mater.*, 2020, **2**, 3643–3649.

S17 L. T. Le, M. H. Ervin, H. Qiu, B. E. Fuchs and W. Y. Lee, *Electrochem. commun.*, 2011, **13**, 355–358.

S18 Y. Xu, M. G. Schwab, A. J. Strudwick, I. Hennig, X. Feng, Z. Wu and K. Müllen, *Adv. Energy Mater.*, 2013, **3**, 1035–1040.

S19 K. Chi, Z. Zhang, J. Xi, Y. Huang, F. Xiao, S. Wang and Y. Liu, *ACS Appl. Mater. Interfaces*, 2014, **6**, 16312–16319.

S20 H. Jung, C. Ve Cheah, N. Jeong and J. Lee, *Appl. Phys. Lett.*, , DOI:10.1063/1.4890840.

S21 M. H. Ervin, L. T. Le and W. Y. Lee, *Electrochim. Acta*, 2014, **147**, 610–616.

S22 Y. Qiu, Y. Zhao, X. Yang, W. Li, Z. Wei, J. Xiao, S. F. Leung, Q. Lin, H. Wu, Y. Zhang, Z. Fan and S. Yang, *Nanoscale*, 2014, **6**, 3626–3631.

S23 J. Qian, H. Jin, B. Chen, M. Lin, W. Lu, W. M. Tang, W. Xiong, L. W. H. Chan, S. P. Lau and J. Yuan, *Angew. Chemie - Int. Ed.*, 2015, **54**, 6800–6803.

S24 G. Yilmaz, C. X. Guo and X. Lu, *ChemElectroChem*, 2016, **3**, 158–164.

S25 W. Liu, C. Lu, H. Li, R. Y. Tay, L. Sun, X. Wang, W. L. Chow, X. Wang, B. K. Tay, Z. Chen, J. Yan, K. Feng, G. Lui, R. Tjandra, L. Rasenthiram, G. Chiu and A. Yu, *J. Mater. Chem. A*, 2016, **4**, 3754–3764.

S26 X. Shi, Z. S. Wu, J. Qin, S. Zheng, S. Wang, F. Zhou, C. Sun and X. Bao, *Adv. Mater.*, 2017, **29**, 1–9.

S27 J. Li, S. Sollami Delekta, P. Zhang, S. Yang, M. R. Lohe, X. Zhuang, X. Feng and M. Östling, *ACS Nano*, 2017, **11**, 8249–8256.

S28 H. Hu and T. Hua, *J. Mater. Chem. A*, 2017, **5**, 19639–19648.

S29 P. Sundriyal and S. Bhattacharya, *ACS Appl. Mater. Interfaces*, 2017, **9**, 38507–38521.

S30 B. Nagar, D. P. Dubal, L. Pires, A. Merkoçi and P. Gómez-Romero, *ChemSusChem*, 2018, **11**, 1849–1856.

S31 Y. Wang, Y. Z. Zhang, D. Dubbink and J. E. ten Elshof, *Nano Energy*, 2018, 49, 481–488.

S32 S. Lochmann, J. Grothe, K. Eckhardt, D. Leistenschneider, L. Borchardt and S. Kaskel, *Nanoscale*, 2018, **10**, 10109–10115.

S33 B. Li, N. Hu, Y. Su, Z. Yang, F. Shao, G. Li, C. Zhang and Y. Zhang, *ACS Appl. Mater. Interfaces*, 2019, **11**, 46044–46053.

S34 B. Duong, Z. Yu, P. Gangopadhyay, S. Seraphin, N. Peyghambarian and J. Thomas, *Adv. Mater. Interfaces*, 2014, **1**, 1–5.

S35 P. Giannakou, M. G. Masteghin, R. C. T. Slade, S. J. Hinder and M. Shkunov, *J. Mater. Chem. A*, 2019, **7**, 21496–21506.

S36 S. Sollami Delekta, K. H. Adolfsson, N. Benyahia Erdal, M. Hakkarainen, M. Östling and J. Li, *Nanoscale*, 2019, **11**, 10172–10177.

S37 J. K. Chih, A. Jamaluddin, F. Chen, J. K. Chang and C. Y. Su, *J. Mater. Chem. A*, 2019, **7**, 12779–12789.

S38 W. Zhao, L. Wei, Q. Fu and X. Guo, *J. Power Sources*, 2019, **422**, 73–83.

S39 H. Li, X. Li, J. Liang and Y. Chen, *Adv. Energy Mater.*, 2019, **9**, 1–13.

S40 Z. Tian, X. Tong, G. Sheng, Y. Shao, L. Yu, V. Tung, J. Sun, R. B. Kaner and Z. Liu, *Nat. Commun.*, 2019, **10**, 1–11.

S41 H. Li, S. Liu, X. Li, Z. S. Wu and J. Liang, *Mater. Chem. Front.*, 2019, **3**, 626–635.

S42 X. Shi, S. Pei, F. Zhou, W. Ren, H. M. Cheng, Z. S. Wu and X. Bao, *Energy Environ. Sci.*, 2019, **12**, 1534–1541.

S43 Y. Wang, Y. Z. Zhang, Y. Q. Gao, G. Sheng and J. E. ten Elshof, *Nano Energy*, 2020, **68**, 104306.

S44 C. W. Wu, B. Unnikrishnan, I. W. P. Chen, S. G. Harroun, H. T. Chang and C. C. Huang, *Energy Storage Mater.*, 2020, **25**, 563–571.

S45 S. Liu, J. Xie, H. Li, Y. Wang, H. Y. Yang, T. Zhu, S. Zhang, G. Cao and X. Zhao, *J. Mater. Chem. A*, 2014, **2**, 18125–18131.

S46 J. M. Munuera, J. I. Paredes, M. Enterría, S. Villar-Rodil, A. G. Kelly, Y. Nalawade, J. N. Coleman, T. Rojo, N. Ortiz-Vitoriano, A. Martínez-Alonso and J. M. D. Tascón, *ACS Appl. Mater. Interfaces*, 2020, **12**, 494–506.

S47 W. He, R. Ma and D. J. Kang, *Carbon N. Y.*, 2020, **161**, 117–122.

S48 B. Li, X. Liang, G. Li, F. Shao, T. Xia, S. Xu, N. Hu, Y. Su, Z. Yang and Y. Zhang, *ACS Appl. Mater. Interfaces*, 2020, **12**, 39444–39454.

S49 W. Zhang, R. Li, H. Zheng, J. Bao, Y. Tang and K. Zhou, *Adv. Funct. Mater.*, 2021, **31**, 1–9.

S50 Y. Brauniger, S. Lochmann, J. Grothe, M. Hantusch and S. Kaskel, *ACS Appl. Energy Mater.*, 2021, **4**, 1560–1567.

S51 J. Diao, J. Yuan, A. Ding, J. Zheng and Z. Lu, *Macromol. Mater. Eng.*, 2018, 303.

S52 Y. Wang, Y. Shi, C. X. Zhao, J. I. Wong, X. W. Sun and H. Y. Yang, *Nanotechnology*, , DOI:10.1088/0957-4484/25/9/094010.

S53 B. Xie, C. Yang, Z. Zhang, P. Zou, Z. Lin, G. Shi, Q. Yang, F. Kang and C. P. Wong, *ACS Nano*, 2015, **9**, 5636–5645.

S54 S. Wang, N. Liu, J. Tao, C. Yang, W. Liu, Y. Shi, Y. Wang, J. Su, L. Li and Y. Gao, *J. Mater. Chem. A*, 2015, **3**, 2407–2413.

S55 H. Pang, Y. Zhang, W. Y. Lai, Z. Hu and W. Huang, *Nano Energy*, 2015, **15**, 303–312.

S56 G. Sun, J. An, C. K. Chua, H. Pang, J. Zhang and P. Chen, *Electrochem. commun.*, 2015, **51**, 33–36.

S57 L. Li, E. B. Secor, K. S. Chen, J. Zhu, X. Liu, T. Z. Gao, J. W. T. Seo, Y. Zhao and M. C. Hersam, *Adv. Energy Mater.*, 2016, **6**, 1–8.

S58 J. Jiang and A. Kucernak, *Electrochim. Acta*, 2002, **47**, 2381–2386.

S59 K. Nam and K. Kim, *J. Electrochem. Soc.*, 2006, **153**, 8–15.

S60 C. Hu, Y. Wu and K. Chang, *Chem. Mater.*, 2008, **20**, 2890–2894.

S61 D. P. Dubal, D. S. Dhawale, R. R. Salunkhe, S. M. Pawar, V. J. Fulari and C. D. Lokhande, *J. Alloys Compd.*, 2009, **484**, 218–221.

S62 H. Jiang, T. Zhao, C. Yan, J. Ma and C. Li, *Nanoscale*, 2010, **2**, 2195.

S63 D. P. Dubal, D. S. Dhawale, R. R. Salunkhe, V. J. Fulari and C. D. Lokhande, *J. Alloys Compd.*, 2010, **497**, 166–170.

S64 D. P. Dubal, D. S. Dhawale, R. R. Salunkhe, S. M. Pawar and C. D. Lokhande, *Appl. Surf. Sci.*, 2010, **256**, 4411–4416.

S65 M. Fang, X. Tan, M. Liu, S. Kang, X. Hu and L. Zhang, *CrystEngComm*, 2011, **13**, 4915.

S66 D. P. Dubal and R. Holze, *J. Power Sources*, 2013, **238**, 274–282.

S67 Y. Li and X.-M. Li, *RSC Adv.*, 2013, **3**, 2398.

S68 L. Wang, L. Chen, Y. Li, H. Ji and G. Yang, *Powder Technol.*, 2013, **235**, 76–81.

S69 J. Liu, Y. H. Ng, M. B. Okatan, R. Amal, K. A. Bogle and V. Nagarajan, *Electrochim. Acta*, 2014, **130**, 810–817.

S70 J. Bhagwan, A. Sahoo, K. Lal and Y. Sharma, *Electrochim. Acta*, 2015, **174**, 992–1001.

S71 D. P. Shaika, P. Rosaiah and O. M. Hussain, *J. Adv. Chem.*, 2015, **12**, 3919–3933.

S72 B. Gnana Sundara Raj, A. M. Asiri, J. J. Wu and S. Anandan, *J. Alloys Compd.*, 2015, **636**, 234–240.

S73 J. Feng, S. Ye, X. Lu, Y. Tong and G. Li, *ACS Appl. Mater. Interfaces*, 2015, **7**, 11444–11451.

S74 Y. Luo, T. Yang, Z. Li, B. Xiao and M. Zhang, *Mater. Lett.*, 2016, **178**, 171–174.

S75 A. A. Yadav, S. N. Jadhav, D. M. Chougule, P. D. Patil, U. J. Chavan and Y. D. Kolekar, *Electrochim. Acta*, 2016, **206**, 134–142.

S76 X. Li, Z. Song, Y. Zhao, Y. Wang, X. Zhao, M. Liang, W.-G. Chu, P. Jiang and Y. Liu, *J. Colloid Interface Sci.*, 2016, **483**, 17–25.

S77 D. P. Shaik, P. Rosaiah and O. M. Hussain, *Mater. Today Proc.*, 2016, **3**, 64–73.

S78 R. A.V. and R. R. M.S., *Appl. Surf. Sci.*, 2017, **403**, 601–611.

S79 D. P. M. D. Shaik, P. Rosaiah, K. S. Ganesh, Y. Qiu and O. M. Hussain, *Mater. Sci. Semicond. Process.*, 2018, **84**, 83–90.

S80 V. Nulu, *Int. J. Electrochem. Sci.*, 2018, **13**, 8313–8321.

S81 R. Tholkappiyan, A. N. Naveen, K. Vishista and F. Hamed, *J. Taibah Univ. Sci.*, 2018, **12**, 669–677.